Loss reduction of abrupt waveguide-bends using Fabry-Perot cavity for optical interconnects

Jau-Jan Deng and Yang-Tung Huang

Department of Electronics Engineering and Institute of Electronics
National Chiao Tung University
1001 Ta-Hsueh Road, Hsinchu, Taiwan, Republic of China

ABSTRACT

A novel low-loss bending structure in dielectric waveguides is proposed. In the proposed structure, an antiresonant Fabry-Perot cavity parallel to the original waveguide is added at the outer side of the bend in order to reduce the bending loss. Based on a simple design rule for the antiresonant cavity, the materials can be flexibly chosen to be adapted to fabrication methods. The beam propagation method is used to verify this low-loss design. The double-bend and curved structures using the same principle for further loss improvement are also presented.

Keywords: Waveguide-bends, Antiresonant Conditions, Optical Interconnects, Fabry-Perot Cavity

1. INTRODUCTION

Waveguide bends are the basic structures for optical interconnects or optical routing in integrated optical circuits. In order to increase packing density in limited chip areas, it is important to find large bending-angle configurations with minimal radiation loss and modal field distortion. In a conventional waveguide structure, the wave is transversely resonant in the guiding region with total internal reflections at interfaces between core and cladding regions. However, when the guided light goes into a bend, phase mismatches happen and the transverse resonance condition no longer holds. Consequently, radiation losses occur at the outer side of the corner after the wave passing the bending region, i.e., the well-guided waves become leaky.

A considerable number of studies have been devoted to analyzing and optimizing the bending structures.[1–9] Compensation of phase-difference of the phase-front,[1–5] coherent coupling of successive connected bends,[6–8] and redirection of radiated waves by an outrigger waveguide[9] are methods commonly used to reduce bending losses. The design of the last two types of bends are cumbersome problems because the coupling of radiation modes are involved. Proposed phase-front compensation methods include decelerating the phase-front inside the abrupt bend,[4] accelerating phase-front outside the an abrupt bend,[5] and adding a microprism in the bend region[1–3] are proposed. In this presentation, a novel waveguide-bend structure without a complex configuration, which can be applied to any material system, is proposed.

In the proposed structure, an antiresonant Fabry-Perot cavity parallel to the original conventional waveguide is added at the outer side of the bend to reduce the radiation loss. Based on the Fabry-Perot interference principle, a design rule for the antiresonant cavity is developed.[10] By raising the reflectance of the Fabry-Perot cavity, the transmission efficiency of a bend will be enhanced. The reflectance of a Fabry-Perot cavity is mainly determined by the differences between the refractive or effective indices of two adjacent regions. The radiation loss predicted by the overlap integral of modal fields between two sections of the bend can confirm the usefulness of this structure. BPM (beam propagation method) simulation is also used to verify the design idea. The double-bend and curved structures using the same principle for further loss improvement are also evaluated.

2. WAVEGUIDE BEND WITH FABRY-PEROT CAVITY CLADDING

The configurations of a conventional abrupt bend and the proposed low-loss bend structure are shown in Figures 1(a) and (b), respectively. Two identical waveguides with different orientations are connected by sharply corner for both cases. α is the bending angle, W is the core width, and n_g, n_c are the refractive indices of the core and the cladding, respectively. In both waveguides discussed in this presentation only one mode is guided.

In the proposed structure, a high-index region with refractive index n_h and width d_h is added to be parallel to the original waveguide at the outer side of the bend to form a Fabry-Perot cavity. Consider a Fabry-Perot cavity as

shown in Figure 2. The reflection coefficients r_{gh} at the interfaces between n_g and n_h, and r_{hc} between n_h and n_c are given as[11]

$$r_{gh} = \frac{\kappa_g - \kappa_h}{\kappa_g + \kappa_h}, \tag{1}$$

$$r_{hc} = \frac{\kappa_h - \kappa_c}{\kappa_h + \kappa_c}, \tag{2}$$

where κ_i represents the transverse propagation constant of the waves in the i-th region. The total reflectance across the high-index cavity is given as

$$R = \left| \frac{r_{gh} + r_{hc} \exp(-i2\kappa_h d_h)}{1 + r_{gh} r_{hc} \exp(-i2\kappa_h d_h)} \right|^2, \tag{3}$$

From the Fabry-Perot cavity interference theory,[11] it can be seen that the reflectance R will reach its peak values when the cavity is at the antiresonance, i.e.,

$$\kappa_h d_h = \frac{\pi}{2}(2P + 1), \tag{4}$$

where $P = 0, 1, 2, \cdots$. In this case, the transmittance through the cavity is thus at its minimum. Moreover, the higher n_h is, the larger and broader the peak value of R is. Thus, if we design a high-index cavity with a larger refractive index, the reflectance of the cavity can remains high even when the width of each region is slightly changed. Figure 3 shows some examples of the reflectance characteristics of this cavity as a function of $\kappa_h d_h$. In the examples, the operating wavelength is $\lambda = 1.5$ μm, $W = 6$ λ, $n_g = 1.502$, and $n_c = 1.5$, and n_h varied with the values of 1.52, 1.55, 1.7, 2.0, 3.0.

Now, a simple design rule for the antiresonant cavity of the proposed low-loss abrupt bend is developed.[10] Because only single TE mode is supported in the core region, the dispersion relation can be simplified as

$$\kappa_g W_{eff} \approx \pi, \tag{5}$$

where the effective width W_{eff} of the core is

$$W_{eff} = W + \frac{1}{\kappa_c}, \tag{6}$$

which takes account of the penetration depth in the cladding region as shown in Figure 4, especially important for weakly guided waves. Combining EqS. (4), (5), and the Snell's law, we can obtain the relation as

$$d_h = \frac{\lambda}{4n_h} \left(1 - \frac{n_g^2}{n_h^2} + \frac{\lambda^2}{4n_h^2 W_{eff}^2} \right)^{-1/2} \cdot (2P + 1), \tag{7}$$

where $P = 0, 1, 2, \cdots$. Based on this design rule, the width of the high-index cavity can be determined whenever the material of each region is chosen.

After the antiresonant Fabry-Perot cavity parallel to the original waveguides is added at the outer side of the bend, the wave is then confined in the core region by the total internal reflections at the inner interface of the bend but antiresonant reflections at the outer interface. According to the above analysis of the Fabry-Perot interference, the ultra-high reflectance at outer interface will hold for a large range of cavity width. Hence, the outer-interface reflectance remains high when the wave pass through the bend region, loss reduction can be expected for this configuration. The reflectance of a Fabry-Perot cavity is mainly determined by the differences between the refractive or effective indices of two adjacent regions. The flexible design rule is, therefore, suitable for all material systems or for rib waveguides by varying the rib thickness or width. Figure 5 shows three possible configurations of the channel waveguides with abrupt bends using antiresonant Fabry-Perot cavity, including ridged-type, buried-type and loaded-type.

3. BENDING LOSS ANALYSIS BASED ON MODE COUPLING AT THE BENDING INTERFACE

To investigate the bending loss improvement of our structure, we analyze the wave propagation and power exchange between the guided and radiation modes based on the theory developed by Taylor.[6] The modal fields of the conventional waveguide and the proposed structure are shown in Figure 6. The coordinate system is shown in Figure 1, and we assume that the fundamental mode with unity power is launched into the first section of the bends. The field at the i-th section can be expanded into a complete set of eigenmodes as

$$f^{(i)}(x^{(i)}, z^{(i)}) = a_g^{(i)} u_g^{(i)}(x^{(i)}) \exp\left[-j\beta_g^{(i)} z^{(i)}\right] + \int a_r^{(i)} u_r^{(i)}(x^{(i)}; \beta) \exp\left[-j\beta z^{(i)}\right] d\beta, \tag{8}$$

where subscripts g, r represent the guided and radiation modes, respectively, $u(x)$ is the normalized field, a is the linear coefficient and β is the propagation constant. In this analysis, the reflected waves are negligible. By applying the field continuity at $\zeta = 0$ plane, where

$$x^{(1)} = \xi \cos(\alpha/2), \tag{9}$$
$$z^{(1)} = \xi \sin(\alpha/2) + l^{(1)}, \tag{10}$$
$$x^{(2)} = \xi \cos(\alpha/2), \tag{11}$$
$$z^{(2)} = -\xi \sin(\alpha/2), \tag{12}$$

and the orthogonal conditions of

$$\int u_\beta(x) u_{\beta'}^*(x) dx = \delta_{\beta\beta'}, \tag{13}$$

we can obtain

$$a_g^{(2)} \tag{14}$$
$$= \cos\frac{\alpha}{2}\, a_g^{(1)} \int u_g^{(1)}\left(\xi\cos\frac{\alpha}{2}\right) u_g^{*(2)}\left(\xi\cos\frac{\alpha}{2}\right) \exp\left[-j\beta_g^{(1)} l^{(1)}\right] \exp\left[-j\,2\,\beta_g^{(1)}\,\xi\sin\frac{\alpha}{2}\right] d\xi \tag{15}$$
$$a_r^{(2)}\left(\beta_r^{(2)}\right) \tag{16}$$
$$= \cos\frac{\alpha}{2}\, a_g^{(1)} \int u_g^{(1)}\left(\xi\cos\frac{\alpha}{2}\right) u_r^{*(2)}\left(\xi\cos\frac{\alpha}{2}\right) \exp\left[-j\beta_g^{(1)} l^{(1)}\right] \exp\left[-j\left(\beta_g^{(1)} + \beta_r^{(2)}\right)\xi\sin\frac{\alpha}{2}\right] d\xi \tag{17}$$

where $a_g^{(1)} = 1, \beta_g^{(1)} = \beta_g^{(2)}$ are presumed before.

Figure 7 (a) shows $a_g^{(2)}$ as a function of the bending angle α with other parameter values as in Figure 3 except for $n_h = 2.0$. Clearly, the excited guided mode at output section is enhanced when the antiresonant Fabry-Perot cavity exists. Figure 7 (b) shows the radiation spectrum at output section when α equals 5°. It can be seen that the amount of output radiation modes of the proposed structure is decreased which can explain the increasing excitation of the guided mode. Thus, lower radiation loss of the proposed structure than the conventional abrupt bend is expectable.

4. DESIGN EXAMPLES AND BPM SIMULATIONS

In this section, we present some design examples and use the standard finite-difference beam propagation method (FDBPM) with transparent boundary condition (TBC) to evaluate the radiation loss of the proposed structure.[12–14]

4.1. Single-Bend Structure

In single-bend structures, we use the same parameter values as in Figure 3, i.e., $\lambda = 1.5$ μm, $W = 6\ \lambda$, $n_g = 1.502$, and $n_c = 1.5$, and n_h varied with the values of 1.52, 1.55, 1.7, 2.0, 3.0. The corresponding d_h are 1.567, 0.970, 0.470, 0.287, and 0.144 μm for $P = 1$, respectively. Figures 8(a) shows the field evolution profiles for the conventional single-bend with an angle $\alpha = 5°$, and (b) for the proposed structures with $n_h = 2.0$ and an angle $\alpha = 12°$. Here, the fundamental mode with a unit power is launched into the straight section of the bends. Obviously, a significant

portion of the incident power is radiated toward the outer-edge of the corner in the conventional bend. In the proposed structure, the additional antiresonant Fabry-Perot cavity can diminish the radiation loss toward this path. Namely, this additional cavity acts like a corner reflector which can more or less reflect the radiated light back into the guiding region. For convenience of discussion, we define the transmission efficiency of the bend η as the overlap integral between the output field and the incident field. In order to reduce the radiation loss and modal field distortion, η should be maintained as high as possible. The calculated η associated with Figure 8 is shown in Figure 9. η decays rapidly along the propagation distance in the conventional case. On the other hand, in the proposed structure, η is firstly decreasing, then increasing to a local maximum and finally decreasing again. This phenomena can be explained from the field evolution profiles shown in Figure 8 (b). From the starting point of the bend, the incident wave gradually shifts to the outer-edge of the corner because of the bending structure. Then the antiresonant cavity reflects the shifted wave toward the inner-edge of the corner. Finally, the wave is radiated toward the inner-edge other than the outer-edge of the corner. As the refractive index of antiresonant cavity increases, the amount of redirected wave field increases, and the cavity acts more like a reflector. For other n_h values, we have the same effects.

4.2. Double-Bend Structure

An double-bend structure is proposed to further reduce radiation loss toward the inner-edge as discussed above. This improved structure is depicted in Figure 10, where $l^{(2)}$ is the length of the connected section. $l^{(2)}$ is chosen to be the length where the transmission efficiency reaches its local maximum as explained above. From a simple geometrical point of view, $l^{(2)}$ can be choose as

$$l^{(2)} = 2W_{eff}\left(\cot\alpha - \frac{1}{2}\csc\alpha\right), \tag{18}$$

where the effective width W_{eff} is defined in Eq. (6). The trace of the wave peak is shown in this figure, which takes advantage of antiresonant cavity as a reflector. The field evolution profile for double-bend structure with $n_h = 2.0$ and total bending angle of $2\alpha = 24°$ and its transmission efficiency is shown in Figures 11(a) and (b), respectively. It can be seen that the transmission efficiency of the improved structure remains high after the shifted wave is reflected back toward the inner-edge of the corner. The applications to Z-bend and Y-junction need further studies.

4.3. Curved-Bend Structure

In addition to the abrupt bend, another choice of bending component is the curved waveguide which is illustrated in Figure 12. In this section, we briefly evaluate the curved structure with a parallel antiresonant Fabry-Perot cavity at the outer side of the bend. The structure parameters chosen here are the same as the reference paper[15] for a comparison with $n_g = 1.503$, $n_c = 1.5$, $\lambda = 1.0\ \mu$m, $W = 4\ \mu$m, and the bending radius $R = 4000\ \mu$m. The additional cavity is set to be $n_h = 1.98$ and $d_h = 0.193\ \mu$m. In order to investigate the bending and transition loss of such waveguides, we adopt BPM which is extensively used to model waveguides with arbitrary curvatures. In the BPM analysis, the index profile of a curved waveguide is transformed to a modified index profile of the equivalent straight waveguide.[16] Because the bending radius is much larger than the core width, the modified index profile $N_E(x)$ can be approximated as

$$N_E(x) = N(x) \cdot \frac{x}{R}, \tag{19}$$

where $N(x)$ is the real index profile of the curved waveguide and x is perpendicular to the core axis from the center of the waveguide. In BPM calculation, a computation window $L_x = 40\ \mu$m with sampling point $N_x = 1000$ and the longitudinal distance $L_z = 3000\ \mu$m with step size $\Delta z = 0.15\ \mu$m is selected. Figure 13(a) and (b) show the modified index profiles and the input and output fields for the conventional case and Figure 14(a) and (b) show those of the proposed curved waveguides, respectively, where we restrict ourselves to the case of TE mode and the normalized fundamental TE_0 mode is excited at input end. A significant power loss in the conventional case and low-loss characteristic of the proposed structure are observed as in the discussion of the abrupt bends. Figure 15 shows the differential power loss which is defined as

$$2\Gamma = -\frac{1}{\Delta z}\ln\frac{P(z+\Delta z)}{P(z)}, \tag{20}$$

where $P(z+\Delta z)$ and $P(z)$ is the total power within the computation window at $z+\Delta z$ and z, respectively. The transition loss which is in rapid fluctuation at a small axial distance in the conventional case seen in Figure 15 is greatly suppressed in the proposed structure. The pure bending loss which is asymptotic at a large axial distance is drastically improved from 1.45×10^{-3} dB/μm in the conventional case to 6.5×10^{-5} dB/μm in the proposed structure.

5. SUMMARY

A novel structure which can reduce the bending loss of dielectric waveguides is proposed. An antiresonant Fabry-Perot cavity parallel to the original waveguides is added at the outer side of the bend to reduce the radiation loss toward the outer-edge of the bend. Based on the Fabry-Perot interference, a simple design rule for the antiresonant cavity is developed. According to BPM analysis, about 90% transmission efficiency can be achieved for a bending angle of 12° at a propagation distance of about 50λ. Furthermore, we propose a double-bend structure which takes advantage of the Fabry-Perot cavity as a corner reflector. The length of the conjunction section between two bends can be chosen by a simple geometrical relation. Based on this configurations, about 80% transmission efficiency can be achieved for a total bending angle of 24° at a propagation distance of about 100λ. We also evaluate the curved waveguides using the same principle. The transition loss is greatly suppressed and the pure bending loss is drastically improved from 1.45×10^{-3} dB/μm to 6.5×10^{-5} dB/μm for the bending radius of 4000 μm. Applications of the presented concept to Z-bend and Y-junction should be a great interest in the future.

ACKNOWLEDGEMENTS

This work was supported by the National Science Council of the Republic of China under contract NSC86-2221-E-009-040.

REFERENCES

1. K. Hirayama and M. Koshiba, "A new low-loss structure of abrupt bends in dielectric waveguides," *J. of Lightwave Technol.*, vol. LT-10, no. 5, pp. 563–569, 1992.
2. S. Safavi-Naeini and Y. L. Chow, "A novel design and analysis of low-loss abrupt bends of dielectric slab waveguides " *J. of Lightwave Technol.*, vol. LT-10, no. 5, pp. 570–580, 1992.
3. H. B. Lin, J. Y. Su, P. K. Wei and W. S. Wang, "Design and application of very low-loss abrupt bends in optical waveguides," *J. of Quantum Electron.*, vol. QE-30, no. 12, pp. 2827–2835, 1994.
4. E. G. Neumann, "Reducing radiation loss of tilts in dielectric optical waveguides," *Electron. Lett.*, vol. 17, no. 5, pp. 369–371, 1986.
5. T. Shina, K. Shiraishi, and S. Kawakami, "Waveguide-bend configuration with low-loss characteristics," *Opt. Lett.*, vol. 11, no. 11, pp. 736–738, 1986.
6. H. F. Taylor, "Power loss at directional change in dielectric waveguides," *Appl. Opt.*, vol. 13, no. 3, pp. 642–647, 1974.
7. L. M. Johnson and F. J. Leonberger, "Low-loss $LiNbO_3$ bends with coherent coupling," *Opt. Lett.*, vol. 8, no. 2, pp. 111–113, 1983.
8. L. M. Johnson and D. Yap, "Theoretical analysis of coherently coupled optical waveguide bends," *Appl. Opt.*, vol. 23, no. 17, pp. 2988–2990, 1984.
9. S. N. Radcliffe and T. P. Yound, "New low-loss bend structures for high-density integrated optical switch arrays," *J. of Select. Area. Commun.*,, vol. 6, no. 8, pp. 1169–1177, 1988.
10. M. A. Duguay, Y. Kokubun and T. L. Koch, "Antiresonant reflecting optical waveguides in SiO_2-Si multilayer structures," *Appl. Phys. Lett.*, vol. 49, no. 1, pp. 13–15, 1986.
11. P. Yeh, *Optical waves in layered media*, chap. 4, John Wiley & Sons, Singapore, 1991.
12. Y. Chung and N. Dagli, "An assessment of finite difference beam propagation method," *IEEE J. Quantum Electron.*, vol. 26, no. 8, pp. 1335–1339, 1990.

13. G. R. Hadley, "Transparent boundary condition for beam propagation," *Opt. Lett.*, vol. 16, no. 9, pp. 624–626, 1991.

14. H. J. W. H. Hoekstra, G. J. M. Krijnen, and P. V. Lambeck, "Efficient interface conditions for the finite difference beam propagation method," *IEEE/OSA J. Lightwave Technol.*, vol. LT-10, no. 10, pp. 1352–1355, 1992.

15. M. Rivera, "A finite difference BPM analysis of bent dielectric waveguides," *IEEE/OSA J. Lightwave Technol.*, vol. LT-13, no. 2, pp. 233–238, 1995.

16. M. Heiblum and J. H. Harris, "Analysis of curved optical waveguides by conformal transformation," *IEEE J. Quantum Electron.*, vol. 11, no. 2, pp. 75–83, 1975.

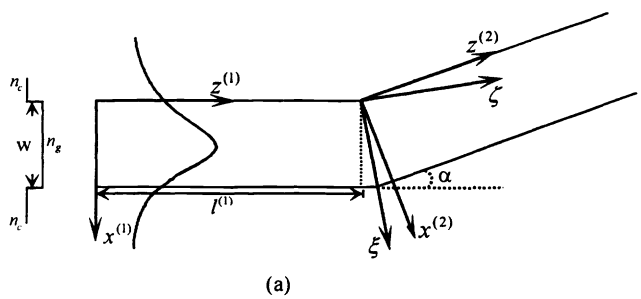

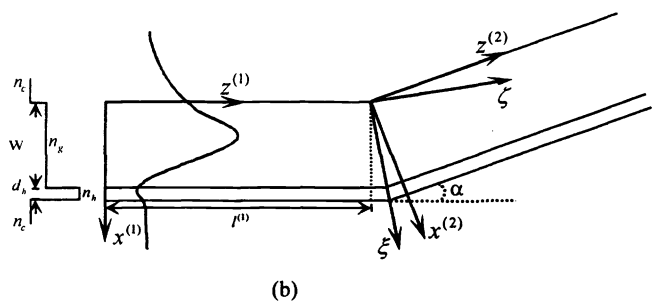

Figure 1. Configuration of abrupt bends: (a) conventional, and (b) proposed structure.

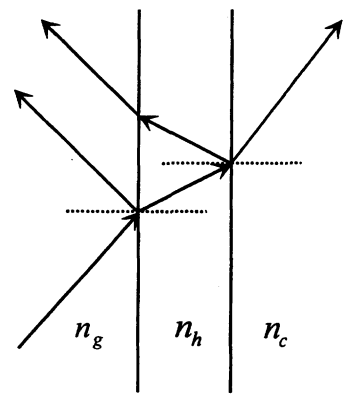

Figure 2. Two interface of a Fabry-Perot cavity.

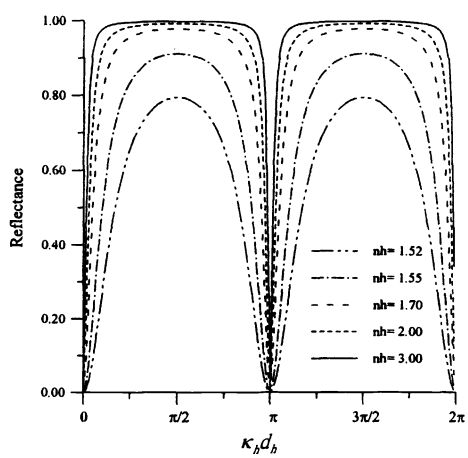

Figure 3. Reflectance of a Fabry-Perot cavity.

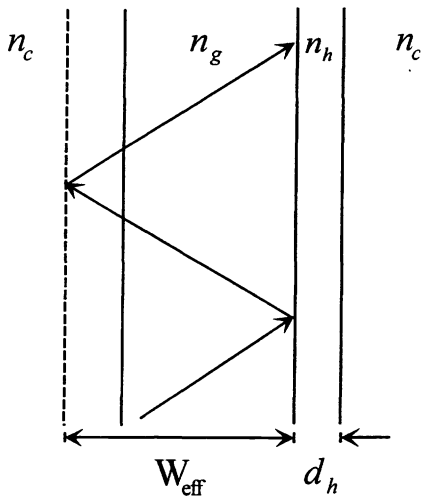

Figure 4. The effective width of the core region.

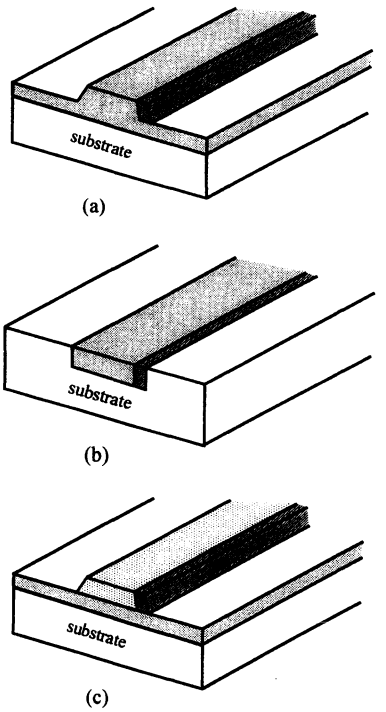

Figure 5. Three dimensional waveguide structures: (a) ridged, (b) buried, and (c) loaded.

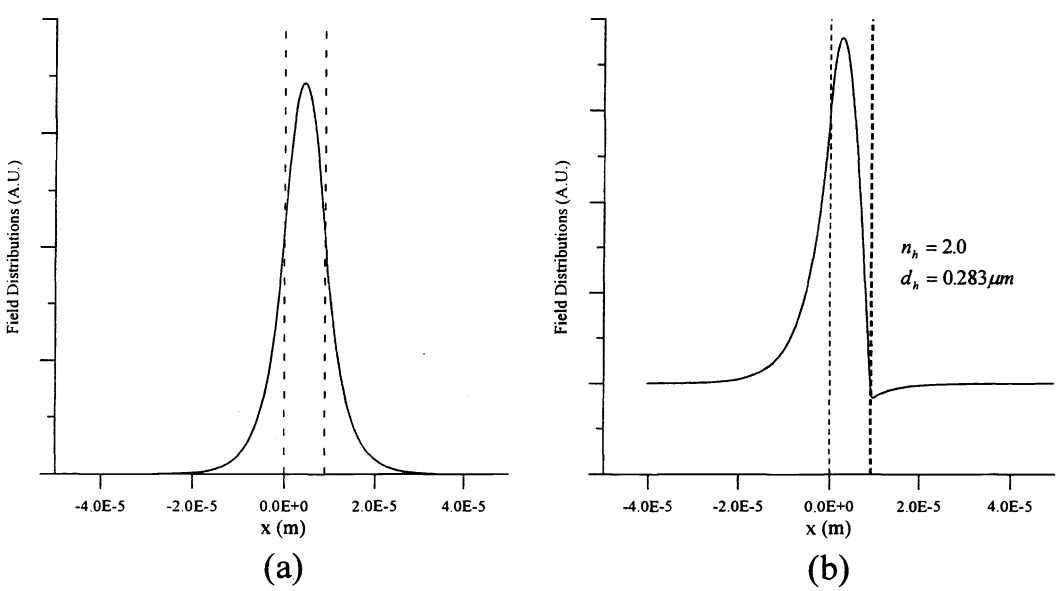

Figure 6. The modal fields of (a) conventional, and (b) proposed structure.

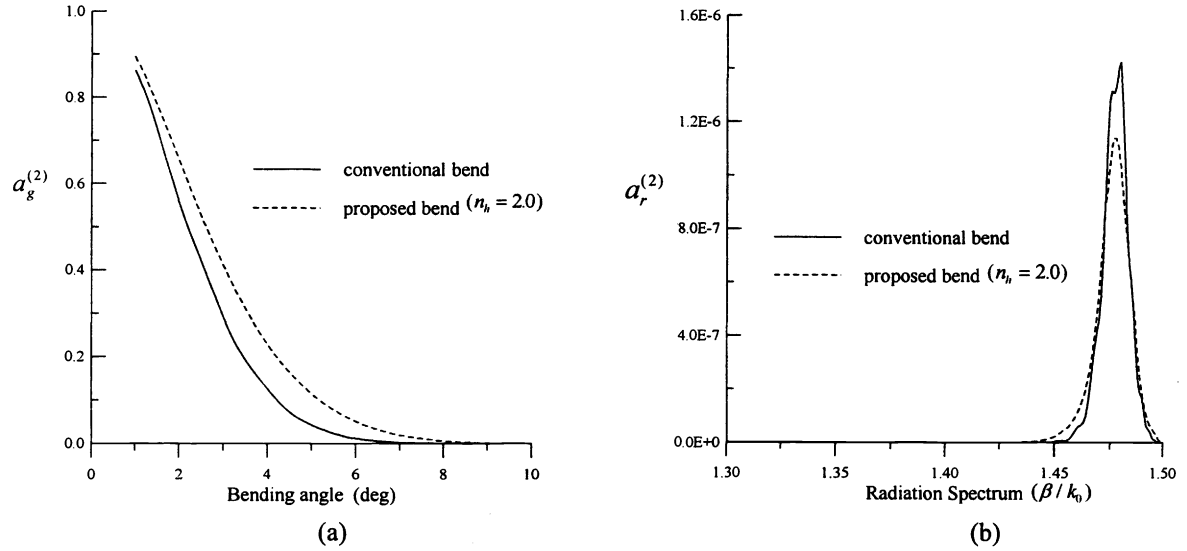

Figure 7. Overlap integrals for conventional and proposed structure: (a) $a_g^{(2)}$ as a function of α , (b) radiation spectrum of $\alpha = 5^{\circ}$.

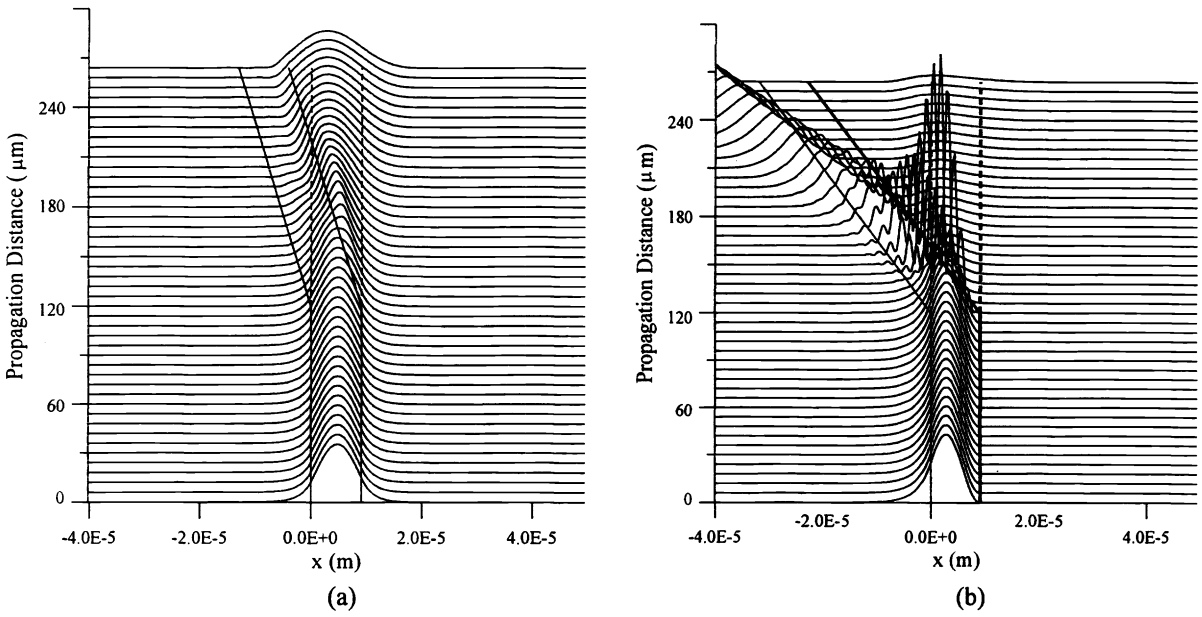

Figure 8. Field evolution profiles for (a) a $\alpha = 5^{\circ}$ conventional bend, and (b) a $\alpha = 12^{\circ}$ bend for the proposed structure with $n_h = 2.0$. The input field is the fundamental mode TE_0 with unit power.

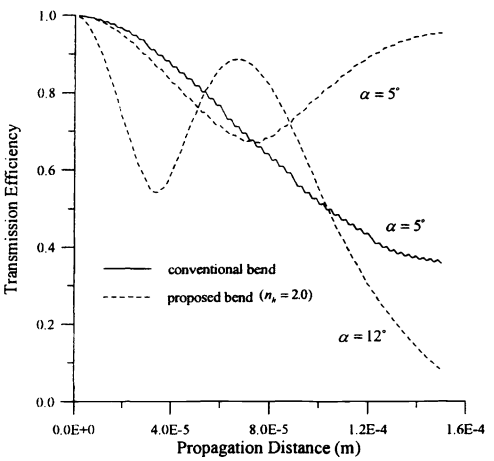

Figure 9. Transmission efficiency η associated with Figure 8.

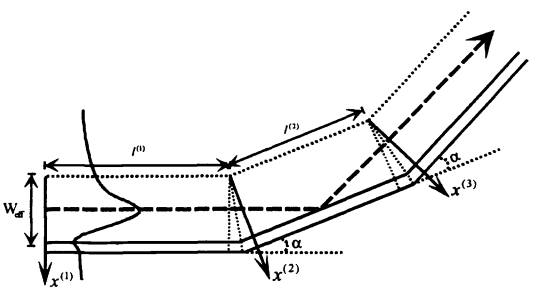

Figure 10. Configuration of the double-bend structure.

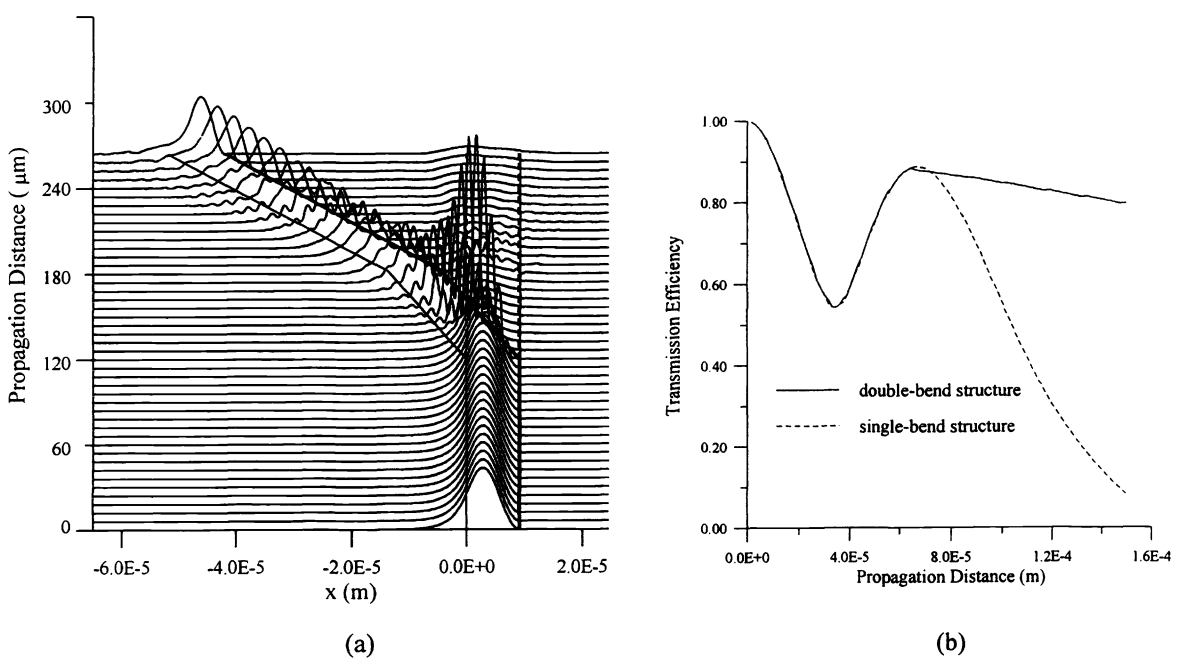

Figure 11. (a) Field evolution profile for the double-bend structure with a total bending angle of $2\alpha = 24°$. (b) The corresponding transmission efficiency η .

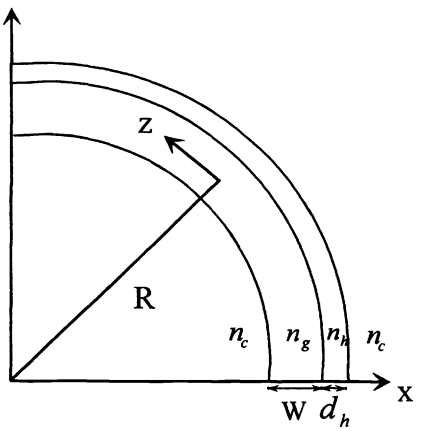

Figure 12. The curved structure.

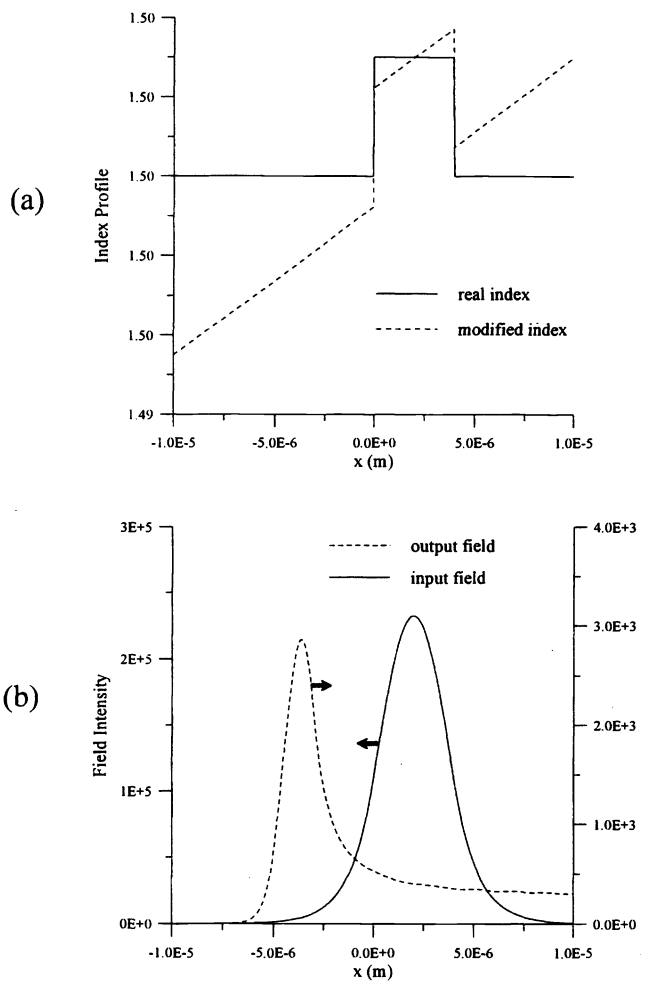

Figure 13. (a) The modified index profile, and (b) the input, output field distributions for the conventional curved waveguides.

(a)

(b)

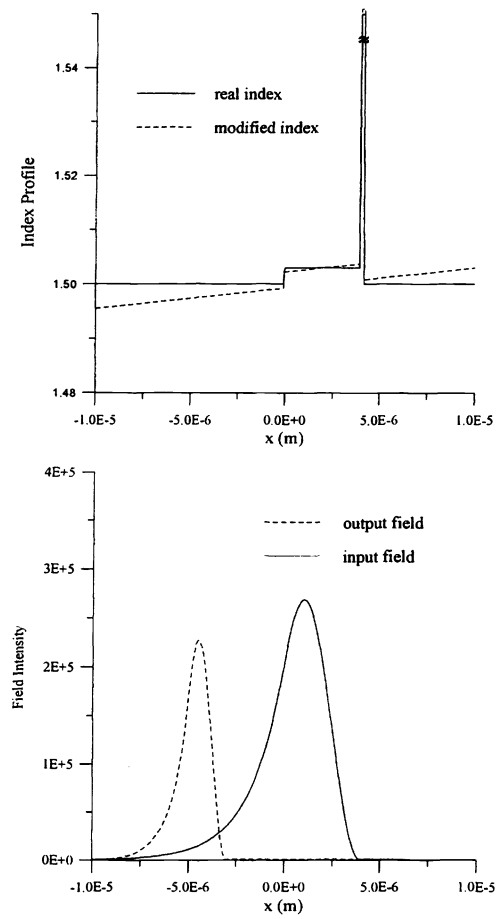

Figure 14. (a) The modified index profile, and (b) the input, output field distributions for the proposed curved waveguides.

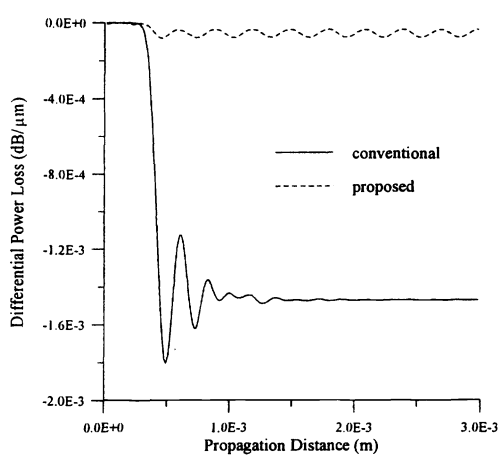

Figure 15. Differential power loss as a function of propagation distance for conventional and proposed curved waveguides.